System and device technologies for coherent optical communications

Kojima, K.; Koike-Akino, T.; Millar, D.S.; Wang, B.; Pajovic, M.; Parsons, K.; Song, B.; Klamkin, J.

Abstract

We review the recent advancement in the system and device technologies for coherent optical communications. One major topic is high-dimensional modulation, and in particular the nonlinearity-tolerant modulation format family, based on four-dimensional 2A8PSK. This family, covering 5, 6, 7 bits/4D symbol, outperforms most known corresponding modulation formats in the linear and nonlinear region. We also review our recent progress on forward error correction including polar codes, and monolithic narrow linewidth semiconductor lasers.

System and device technologies for coherent optical communications

Keisuke Kojima[a], Toshiaki Koike-Akino[a], David S. Millar[a], Bingnan Wang[a], Milutin Pajovic[a], Kieran Parsons[a], Bowen Song[b], and Jonathan Klamkin[b]

[a]Mitsubishi Electric Research Laboratories, 201 Broadway, Cambridge, MA 02139 USA
[b]Electrical and Computer Eng. Dept., University of California, Santa Barbara, CA 93106, USA

ABSTRACT

We review the recent advancement in the system and device technologies for coherent optical communications. One major topic is high-dimensional modulation, and in particular the nonlinearity-tolerant modulation format family, based on four-dimensional 2A8PSK. This family, covering 5, 6, 7 bits/4D symbol, outperforms most known corresponding modulation formats in the linear and nonlinear region. We also review our recent progress on forward error correction including polar codes, and monolithic narrow linewidth semiconductor lasers.

Keywords: Optical coherent communications, high-dimensional modulation, FEC, laser

1. INTRODUCTION

Due to the progress of digital signal processing (DSP) used in coherent optical transmission systems, there is increasing interest in more advanced modulation formats for larger spectral efficiency, finer spectral efficiency granularity, and higher tolerance to fiber nonlinearity.[1,2] Multidimensional coded-modulation, where more than two-dimensions are utilized, is one of the most powerful ways of achieving these characteristics. In Sec. 2, we review the coded-modulation approach for multidimensional modulation, and show its benefit on additive white Gaussian noise (AWGN) channels. In Sec. 3, we overview a special type of 4D coded-modulation, called 4D-2A8PSK. It can offer three different spectral efficiencies covering 5, 6, 7 bits/4D symbol, having 4D constant modulus property to achieve excellent fiber nonlinearity tolerance.

We then discuss the recent advances of forward error correction (FEC), with focus on the low-density parity check (LDPC) codes and the emerging polar codes in Sec. 4. Narrow linewidth laser technologies will be also discussed in Sec. 5.

2. MULTIDIMENSIONAL CODED-MODULATION

A multidimensional coded-modulation system is shown in the schematic in Fig. 1.[3] A stream of data from the source is encoded by an outer encoder. The encoded symbol stream is then mapped to multidimensional symbols, on the optical carrier. This block may involve several sub-blocks in specific implementations, such as an inner encoder, followed by a bit-to-field mapping such as a binary phase-shift keying (BPSK) mapper, and then a mapping of BPSK symbols to multiple orthogonal field components and time slots. The multidimensional signal is then sent via the channel to the multidimensional de-mapper. The de-mapped data stream is then decoded by the outer decoder, with optional feedback to the multidimensional de-mapper (turbo-demodulation), before being sent to the sink. The de-mapper may output soft or hard decisions, and may be based on a maximum-likelihood de-mapper or its reduced-complexity variant.[4]

While there are a multitude of methodologies for designing a multidimensional modulation scheme, there are several methods which are particularly well explored. Sphere-packing formats are designed with the optimal arrangement of hyperspheres inside a larger hypersphere of the same dimension,[2] in order to maximize the minimum distance between hypersphere centroids. This is a well-explored mathematical problem, and several
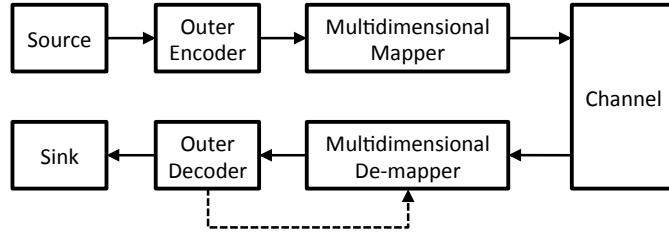
Figure 1. Schematic showing a generic multidimensional coded-modulation system. The dashed line between the outer decoder and multidimensional de-mapper represents optional turbo-demodulation.[3]

optimal solutions are known for particular numbers of dimensions and constellation points. These formats require an optimized bit-to-symbol mapping when the channel code used does not have the same cardinality as the modulation format. For sphere-packing formats, this is often not a significant problem, as the optimal mapping can be computed by brute force in cases with relatively low cardinality, such as those where optimal sphere-packings are known.

Sphere cutting formats are based on the cutting of a subset of points lying within the hypersphere on a lattice which is the optimal sphere-packing lattice in a given number of dimensions.[5,6] Again, some lattices are proven to be optimal in certain numbers of dimensions. These formats also require an optimized bit-to-symbol mapping, which can be problematic in the case where the cardinality of the format is large, and brute force computation quickly becomes impossible. For example, the format based on the selection of 2^{12} points from the Leech lattice (which is known to be the optimal packing in 24 dimensions[7]) has a total number of labelings of $(2^{12} - 1)!$, which (using Stirling's approximation) gives on the order of $10^{13,000}$ unique labelings. In cases where brute force labeling optimization is impossible, numerical techniques such as bit-flipping are often used,[8] although it is worth noting that these numerical methods cannot be guaranteed to reach a global optimum.

The most popular method for designing modulation formats relies on the use of an inner block code,[5,9,10] with a separate mapper to map encoded bits to the optical field. These block coded solutions are particularly interesting, as they can provide codewords with optimal spacing in Hamming distance, while using a simple mapper to the optical field, which has few levels (thus reducing required hardware complexity).

In the very high signal-to-noise ratio (SNR) regimes, the minimum Euclidean distance $d_{\min}$ between constellation points determines the symbol error rate (SER) as the nearest neighbor errors become dominant. One commonly used parameter to quantify the asymptotic noise performance is the sensitivity penalty $1/\gamma$ where γ is the asymptotic power efficiency. Note that for 1 bit/symbol/dimension case of dual-polarization quadrature PSK (DP-QPSK), $\gamma = 1$, hence sensitivity penalty can also be considered as the performance penalty with respect to DP-QPSK for asymptotically high SNR.

In Fig. 2, sensitivity penalty and spectral efficiency of various high-dimensional modulation (HDM) formats obtained by sphere-cutting and block-coding approaches are shown. Here, N is the constellation dimension, and M is the number of constellation points. It can be observed that optimized sphere-cut constellations with 1 bit/symbol/dimension spectral efficiency yield 0, -0.82, -1.87, -2.80 and -4.25 dB sensitivity penalties for $N = 2$, 4, 6, 8 and 16, respectively. In Ref. 2, it is shown that highest power efficiency for $N = 2$ is obtained for $M = 3$ and for $N = 3$ for $M = 4$, both using simplex configurations, i.e. same length vectors with same angular separation. For $N > 3$, simplex configurations are not optimal constellations in terms of power efficiency. For $N = 4$, the highest power efficiency is obtained for $M = 8$, with the 3b-4D polarization-switching (PS) QPSK constellation. Among the values we consider for sphere-cut constellation design, for $N = 6$, 8 and 16, we observe the highest power efficiencies for $M = 2^4$, 2^4 and 2^{11} (4b-6D, 4b-8D and 11b-16D modulation formats). Comparison of modulation formats at lower SNR regimes are discussed in detail in Ref. 5.

3. OPTICAL NONLINEARITY MITIGATING FORMATS

When designing formats for use on nonlinear optical links, a gain can be demonstrated by using formats which minimize this optical nonlinearity. This is particularly prominent for links with low accumulated chromatic
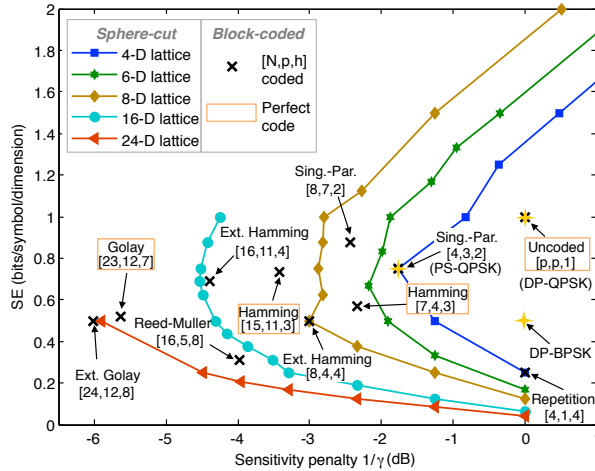
Figure 2. Spectral efficiency (bit/symbol/dimension) vs sensitivity penalty (dB) of optimized sphere-cut constellations (circles) and block-coded modulation (crosses) and commonly used optical modulation formats (stars).[5]

dispersion (CD), such as legacy submarine links. In particular, polarization-managed formats (which seek to minimize the effect of cross-polarization modulation – XPolM),[11] and formats with a constant modulus (which seek to minimize the effects of self- and cross-phase modulation – SPM and XPM)[12] have proven particularly successful. In this section, we review the latter type, i.e., a family of constant modulus formats, called 4D-2A8PSK, for the spectrum efficiency of 5, 6, and 7 bits/4D symbol. These modulation formats are examples of multidimensional block-coded modulation formats as explained in Sec. 2

3.1 Generalized mutual information (GMI)

Conventionally, pre-FEC bit error ratio (BER) has been used to predict post-FEC BER performance of hard decision (HD) FEC systems. On the other hand, for soft-decision (SD) FEC coding based on bit-interleaved coded modulation (BICM), the so-called generalized mutual information (GMI) is a better metric for comparing multiple modulation formats.[13,14] The normalized GMI can be obtained from the log-likelihood ratio (LLR) outputs of the demodulator at the receiver as follows:[15–17]

$$I = 1 - \mathbb{E}_{L,b} \left[\log_2 \left(1 + \exp \left((-1)^{b+1} L \right) \right) \right], \tag{1}$$

where b, L, and $\mathbb{E}[\cdot]$ denote the transmitted bit $b \in \{0, 1\}$, the corresponding LLR value, and an expectation (i.e., ensemble average over all LLR outputs L and transmitted bits b), respectively. We denote "normalized" GMI as the mutual information per modulation bit, not per modulation symbol. The normalized GMI can thus determine the maximum possible code rate of SD-FEC coding for BICM systems. We primarily use the target GMI of 0.85, corresponding to the typical Q^2 threshold of the state-of-the-art SD-FEC having a code rate of 0.8.[18]

3.2 4D-2A8PSK family modulation format

The generic constellation of 4D-2A8PSK is shown in Fig. 3[12]. It is similar to 8PSK, with two different amplitudes represented by the radii, r_1 and r_2 (suppose $r_1 \leq r_2$ without loss of generality). By combining the two polarizations (i.e., 4D space), $2^8 = 256$ combinations (i.e., 8 bits per 4D symbol) are possible. With a condition that X- and Y-polarizations have complimentary radius, i.e., if r_1 is used for X-polarization, then r_2 needs to be chosen for Y-polarization, and vice versa, we generate set-partitioned (SP) 4D codes, achieving the property of 4D constant modulus, which leads to excellent nonlinear transmission performances. Let $B[0], \ldots, B[7]$ express eight modulation bits, and $B[0]$–$B[2]$ and $B[3]$–$B[5]$ denote the Gray-mapped 8PSK at X- and Y-polarizations, respectively. Whereas, $B[6]$ and $B[7]$ are used to express the amplitude in each polarization. By selecting the

optimum 32, 64, and 128-point constellations out of 256 combinations, we can construct 32SP-, 64SP-, and 128SP-2A8PSK, for the spectral efficiency of 5, 6, and 7 bits/symbol, respectively. We also call these 5b4D-, 6b4D-, and 7b4D-2A8PSK for convenience.
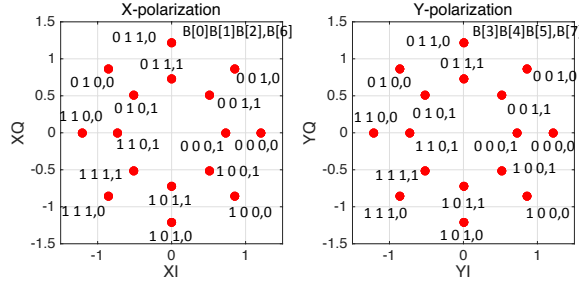

Figure 3. Constellation and bit-to-symbol mapping of 2A8PSK.[12]

3.3 Nonlinear transmission simulation

Nonlinear transmission simulations are conducted over a 2,000 km dispersion-managed (DM) link at a rate of 34 GBaud per channel to evaluate the effect of modulation format on high fiber nonlinearity. At the transmitter, pulses were filtered by a root-raised-cosine (RRC) filter with a roll-off factor of 10%. Eleven dense wavelength-division multiplexing (DWDM) channels of the same modulation format were combined with 37.5 GHz spacing without using any optical filtering. The link consists of 25 spans of 80 km non-zero dispersion shifted fiber (NZDSF) in which loss is compensated by Erbium-doped fiber amplifiers (EDFAs). The performance of each modulation format can be quantified by a span loss budget.[19] The detailed simulation procedure is summarized in Ref. 20

Four 6 bits/symbol modulation formats are compared as in Fig. 4. The optimal ring ratio is $r_1/r_2 = 0.65$ for 6b4D-2A8PSK for maximum span loss budget. The maximum span loss budget for 6b4D-2A8PSK is shown to be higher than DP-Circular-8QAM, DP-8PSK, and DP-Star-8QAM by 0.6 dB, 0.5 dB, and 1.6 dB, respectively.

The peak span loss budget for the DM link is summarized in Fig. 5. The circles connected by the dashed lines include DP-QPSK, 5b4D-, 6b4D-, 7b4D-2A8PSK, and DP-16QAM, all at 34 GBaud. Squares are taken from time-domain hybrid (TDH) modulation formats involving DP-QPSK, 6b4D-2A8PSK, and DP-16QAM, and triangles are from other (conventional) modulation formats, such as 32SP-16QAM, DP-Star-8QAM, and 128SP-16QAM.[21] This shows that the 4D-2A8PSK family fills the gap between DP-QPSK and DP-16QAM almost linearly (in the dB scale), and each one offers a good improvement from the conventional modulation formats at the same spectral efficiency.

3.4 Experiment

We have also conducted a transmission experiment comparing 6b4D-2A8PSK and DP-Star-8QAM.[4] The signals were modulated at 32 GBaud and filtered with an RRC filter with a roll-off factor of 0.15. 70 channels were spaced at 50 GHz spacing. The transmission line was 1,260 km, having an average span length of 70 km. CD was managed in-line by the mixture of NZDSF having negative local CD of -3 ps/nm and standard single-mode fibre (SSMF). In the receiver side, the signal was processed offline, which included CD compensation, adaptive equalization, carrier recovery with multi-pilot algorithm,[22] pilot-aided phase-slip recovery, and soft-demapping. For SD-FEC, it is necessary to calculate LLR with moderate circuit complexity. The proposed soft-demapping uses a fast-decoding algorithm and LLR-computation for high-order SP 4D-QAM formats,[23] extended to 6b4D-2A8PSK to use two lookup tables.[4]

Figure 7 shows the experimental results; Fig. 7 (a) is Q calculated from GMI as a function of launched power. In the case of ideal soft-demapping, we observed 0.6 dB improvement at maximum Q by 4D-2A8PSK compared to DP-Star-8QAM. The proposed technique had performance degradation of 0.15 dB and 0.06 dB for
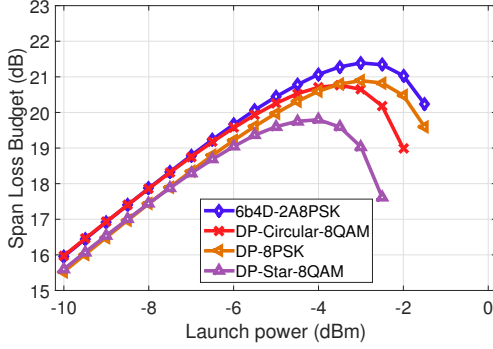
Figure 4. Span loss budget of four 6 bits/symbol modulation formats for the DM link.[20]
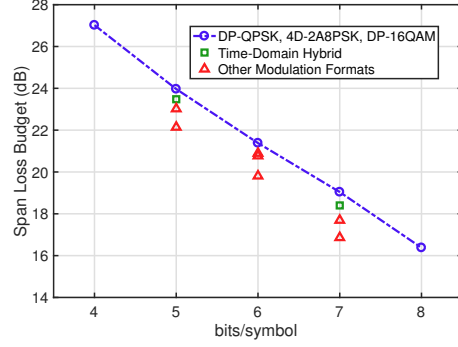

Figure 5. Peak span loss budget for the 2,000 km dispersion managed link. Blue circles are for the three 4D-2A8PSK formats, DP-QPSK, and DP-16QAM. Green squares are for TDH modulation, and red triangles are for other conventional modulation formats.[20]

4D-2A8PSK and DP-Star-8QAM, respectively, compared to the ideal LLR. The overall performance gain of 0.5 dB was still significant in the highly nonlinear transmissions. Fig. 7 (b) shows required optical SNR (OSNR), which was calculated by loading noise at the receiver DSP to emulate OSNR decrease. The target normalized GMI was set to 0.92, which was close to 20.5% SD-FEC limit.[24] The proposed soft-demmaping worked even at such low OSNR conditions and 4D-2A8PSK outperformed DP-Star-8QAM as the launched power increases.
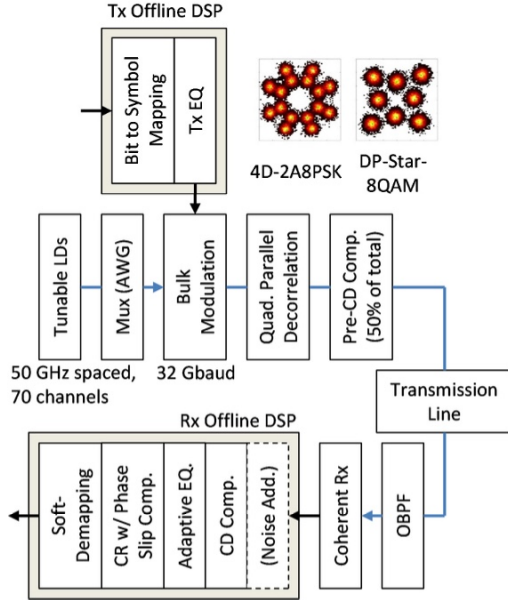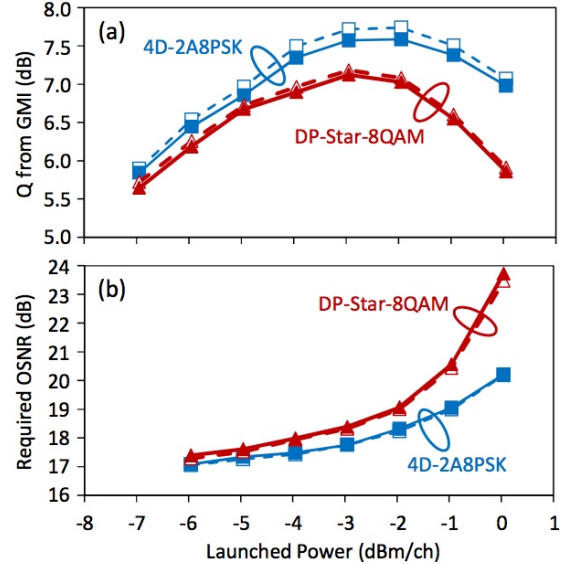

Figure 6. Experimental setup.[4]

Figure 7. Experimental result of (a) Q from GMI and (b) required OSNR for two types of LLR calculation: ideal (dotted line) and the proposed soft-demapping (solid line).[4]

3.5 Time-domain hybrid (TDH) modulation

TDH modulation has been studied considerably to cover a wide range of channel conditions, due to its flexibility in choosing the nearly arbitrary spectral efficiency.[25, 26] As the constituent modulation formats, we use DP-QPSK (4 bits/symbol) and QP-16QAM (8 bits/symbol) in conjunction with 5b4D, 6b4D, and 7b4D-2A8PSK to widen the range of TDH.[27] For a comparison, we also use TDH modulation using conventional modulation formats, i.e., DP-QPSK, 32SP-QAM, DP-Star-8QAM (S8QAM), 128SP-QAM, and DP-16QAM. The benefit of

the 4D-2A8PSK family is the 4D constant modulus property. In other words, there is no compromise in choosing the power ratio (ratio between the two modulation formats). On the other hand, conventional formats experience power fluctuations, causing compromise in the power ratio.[27]

Nonlinear transmission simulations were conducted with the same link condition as described in Sec. 3.3. For 5b4D, 6b4D, and 7b4D-2A8PSK formats, we choose the ring ratio of 0.60, 0.65, and 0.59 for the best nonlinear performance. For all the TDH modulation, we use 1:1 ratio with alternating formats, however, in actual systems, any arbitrary ratio can be used. The important parameter for TDH is the power ratio, i.e., how much power will be allocated for each time slot. The power ratio was optimized for the best nonlinear performance.

The peak span loss budget for various spectral efficiency is shown in Fig. 8. Here, 4.5, 5.5, 6.5, 7.5 bits/symbol TDH based on 2A8PSK used DP-QPSK, 5b4D-2A8PSK, 6b4D-2A8PSK, 7b4D-2A8PSK, and DP-16QAM. TDH based on the conventional formats used DP-QPSK, 32SP-QAM, S8QAM, 128SP-QAM, and DP-16QAM. We observed 1.3, 1.6, 1.6, and 0.6 dB increase in peak span loss budget, when TDH used 2A8PSK, at 4.5, 5.5, 6.5, and 7.5 bits/symbol, respectively. This shows the versatility of the 4D-2A8PSK family.
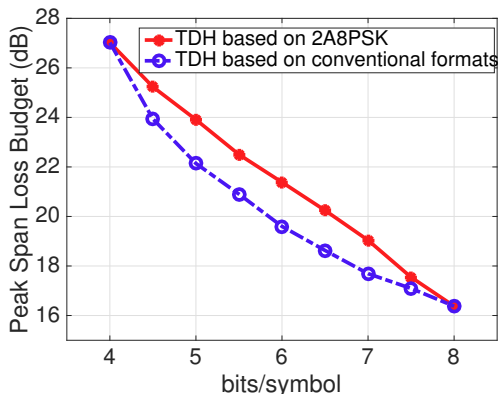

Figure 8. Span loss budget for TDH modulation based on the 4D-2A8PSK formats, and that on the conventional modulation formats.[27]

4. FORWARD ERROR CORRECTION

The most optical communications call for advanced FEC to realize ultra-reliable data transmission achieving a BER below 10^{-15}. In particular, SD-FEC based on low-density parity-check (LDPC) coding[18, 28–34] has played an important role in advancing the lightwave systems by enhancing tolerance against linear and nonlinear fiber distortion. Although well-designed LDPC codes already promised an excellent performance close to channel capacity decades ago,[28] there still exist remaining challenges stemming from stringent hardware specifications in power consumption, latency and throughput for Tb/s-class optical communications. This section reviews recent research topics of hardware-friendly LDPC codes. In addition to LDPC codes, we also review an alternative FEC trend based on polar codes.

4.1 Low-density parity-check (LDPC) codes

Since transceivers for optical communications require high-speed operations to accommodate tens/hundreds of Gb/s or even beyond Tb/s, lower-power processing has been of great importance with a limitation in decoding iteration, computational complexity, memory size, latency, and precision. In Table 1, some potential solutions are listed to deal with various hardware/system issues underlying LDPC deployment. In this subsection, we present selected topics among them, particularly focusing on how to optimize a trade-off between coding gain and computational complexity as well as latency.

LDPC for limited-iteration decoding: The decoding performance of belief propagation (BP) for irregular LDPC codes highly depends on the degree distribution,[28] which can be designed by extrinsic information transfer (EXIT) chart.[15] However, the conventional curve-fitting approach[15] does not take care of a finite number of iterations for BP decoding, which is often significantly limited (e.g., less than 10 times) for high-throughput

Table 1. Challenges in hardware-friendly LDPC codes for high-speed optical communications.

Specification	Potential solutions
High coding gain	Irregular, multiedge,[35] EXIT,[15] generalized,[36] nonbinary,[30–32] BICM-ID[34]
Low-complexity operation	Offset min-sum, delta-min,[37] ultra-sparse[38]
Low error floor	Girth design,[39,40] finite geometry,[41] perturbation, non-BP decoding,[42,43] concatenation
Finite-precision operation	Mixed log/probability, look-up table design[44]
Structured parallelism	Quasi-cyclic, protograph
Low latency	Spatial coupling, LDPC-CC (windowed decoding,[45] tail-biting), short-length design
Low power consumption	Few-iteration,[33] early stopping, dynamic layered scheduling[29,46]
High throughput	Unrolling, pipeline, massive parallel, analog decoding
Rate adaptation	Rate compatible,[47] puncture, shortening, row-splitting,[48] adaptive modulation[49]

and low-power optical transports. Is a certain LDPC code designed at infinite iterations still optimal when few-iteration decoding is carried out to adjust power consumption? No, unfortunately. We have improved the EXIT-based design method of LDPC degree optimization for few-iteration BP decoding,[33,34] and found that the degree distribution should be refined depending on the number of iterations to minimize the performance penalty due to limited BP iterations from the Shannon limit. The design method was originally based on flooding scheduling and later extended to layered scheduling[50] for further improvement. The benefit of the proposed design method is depicted in Fig. 9, where the decoding threshold (i.e., required SNR to asymptotically achieve zero error) is present as a function of the number of decoding iterations for the conventional curve-fitting design and iteration-dependent design methods with flooding or layered scheduling. It is observed that the conventional method approaches the Shannon limit when a large number of BP iterations (more than 30) is available, whereas the huge penalty appears in the few-iteration regimes. The iteration-dependent LDPC optimization can significantly improve the threshold by up to 2 dB for such conditions.
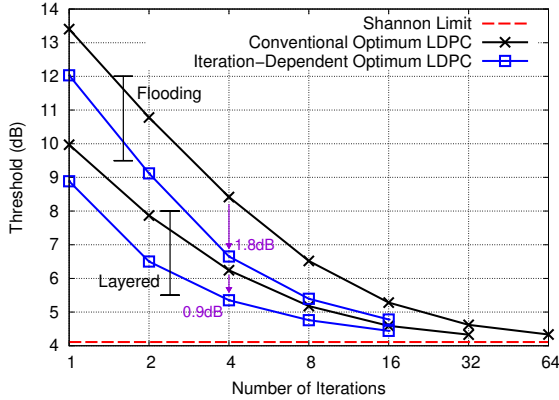

Figure 9. Threshold across BP decoding iteration for iteration-dependent irregular LDPC codes (code rate: 0.8).
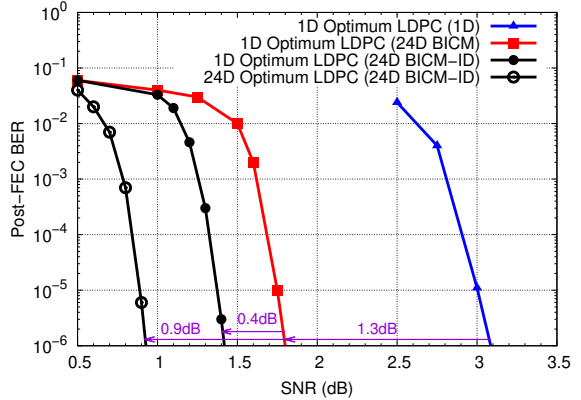

Figure 10. Modulation-dependent irregular LDPC codes for 24D modulation[51,52] with BICM-ID; (code rate: 8/9).

LDPC to minimize complexity: Each curve in Fig. 9 also indicates that higher complexity is usually required to improve performance. Nevertheless, the computational complexity per iteration can be further reduced by sparsifying the degree like ultra-sparse LDPC[38] whose variable node degree is two (i.e., minimum possible value). Since optimized LDPC codes in Fig. 9 have relatively high degree ($\bar{d}_v \geq 4$),[33] we have a possibility to further improve the performance without increasing the total computational complexity by slightly increasing the number of iterations while sparsifying the degree. In order to jointly minimize the required SNR and the computational complexity, another design concept with multi-objective Pareto optimization was introduced[33] by accounting for the average degree in addition to the number of iterations. The Pareto-optimal LDPC codes[33] offer the best trade-off between the complexity and the coding gain, achieving an additional gain by up to 2 dB and a reduced complexity by up to 50% compared to the iteration-dependent LDPC codes.

LDPC for multidimensional modulation: As discussed in Sec. 2, further performance improvement can be provided by introduction of HDM, which directly increases the minimum Euclidean distance by extending the modulation dimension. Is an LDPC code optimized at binary-input AWGN (biAWGN) channels still optimal when we employ HDM? Yes, for the standard bit-interleaved coded-modulation (BICM) systems. However, the BICM is suffered from the fundamental loss, which can be mitigated by means of iterative demodulation (BICM-ID).[34] For BICM-ID, the degree distribution of LDPC codes shall be different for different modulation. We demonstrated that the modulation-dependent optimal LDPC codes can offer additional gain up to 0.5 dB,[34] as illustrated in Fig. 10. The 24D modulation[51,52] itself improves the performance by 1.3 dB from the conventional 1D modulation (BPSK) when we use the standard BICM with an LDPC code optimized at biAWGN channels. However, this optimal LDPC code does not perform well when we employ BICM-ID; specifically, the gain by BICM-ID is limited to 0.4 dB. In order to exploit the full potential of HDM, we shall use another LDPC code optimized for the 24D modulation. The 24D-optimal LDPC code can achieve a significant gain of 0.9 dB by BICM-ID in comparison to BICM.

LDPC for higher gain: BICM-ID requires labeling optimization and a soft-decision feedback from FEC decoder to demodulator. Hence, BICM-ID is often thought of less practical due to the high complexity and large latency. This turbo demodulation can be avoided by using nonbinary (NB)-LDPC codes.[30,31] This is a great advantage of NB-LDPC compared to BICM-ID for hardware implementation. Nonetheless, the major obstacle lies in the fact that the decoder complexity increases linearly with the Galois field size. This complexity issue may be mitigated by an introduction of LDPC convolutional codes (LDPC-CC) with windowed decoding (WD).[45] We demonstrated[32] that a significant performance gain can be obtained by NB-LDPC-CC for HDM, even better than BICM-ID. In addition, the use of LDPC-CC can facilitate low-latency decoding via WD.

LDPC for latency constraint: In order to minimize the decoding latency, we need to reduce the window size and iteration count per WD for LDPC-CC. For such short window cases, layered scheduling needs to be carefully designed to exploit the benefit of LDPC-CC. We have developed a greedy scheduling optimization method based on protograph-based EXIT chart for LDPC-CC,[29] achieving greater than 1 dB gain over the conventional Round–Robin scheduling for 1-iteration layered WD. It was also found that irregular LDPC-CC is not always better than regular LDPC-CC for few-iteration WD. Another advantage of LDPC-CC based on quasi-cyclic (QC) protograph includes its structural homogeneity, facilitating efficient parallel hardware implementation and simple girth design.[39] The scheduling design method can be readily extended to NB-LDPC-CC.[31]

4.2 Polar codes

In principal, the most random codes are known equally good when the block length is large enough. However, the decoding latency is usually increased with the block length. Hence, how to design short LDPC codes has been one of challenging problems for decades. Unfortunately, LDPC codes generally do not perform well at short block lengths. From this reason, the fifth-generation wireless standard has chosen an alternative FEC code based on polar codes[53] besides LDPC codes for short-packet transmission. Among other FEC schemes such as turbo convolutional codes, turbo product codes, tail-biting convolutional codes, repeat-accumulate codes, staircase codes, braided codes, and BCH codes, the polar codes have recently drawn much attention to telecommunication researchers/engineers owing to its theoretical and practical strength. Here we introduce our research activities[50,54] to improve the performance of polar codes in high-throughput optical communications.

Polar for multi-level modulation: Polar codes were proven by Arıkan[53] in 2009 to achieve capacity over any arbitrary discrete-input memoryless channels, without relying on randomness of code construction. However, in spite of theoretical strength, polar codes have not been adopted in practical systems until recently due to their poor performance at short block lengths. A major breakthrough was given in 2015 when Tal and Vardy[55] introduced successive cancellation list (SCL) decoding plus cyclic redundancy check (CRC) to make polar codes competitive with the state-of-the-art LDPC codes. However, the conventional polar code construction assumes memoryless identical channel reliability, which is often not valid, e.g., when we use high-order QAM formats having different reliability across the most to least significant bit-planes. In consequence, careful interleaver design which properly maps the coded bits to modulation bit-planes becomes important not to destruct the so-called channel polarization phenomenon. We have optimized[50] an interleaver parameter for hardware-efficient quadratic polynomial permutation (QPP), achieving more than 0.5 dB gain than random interleaving. The

benefit of interleaver design is shown in Fig. 11, where the SCL decoder performance of $(1024, 828)$ polar coding (with CRC-8 and list size of 32) is present for 256QAM scheme. It is seen that more than 1 dB difference is incurred by good and bad interleaving because polarization phenomenon is greatly affected by bit mapping. We have further improved the performance by introducing a super-Gaussian constellation shaping.[56]
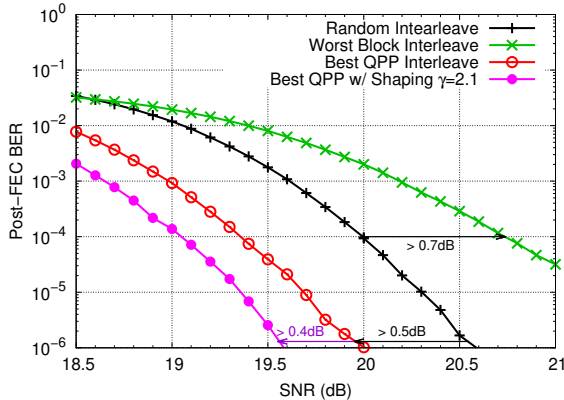

Figure 11. Bit-interleaved polar-coded 256QAM modulation ($L = 32$, CRC-8, $N = 1024$, code rate: 0.8).
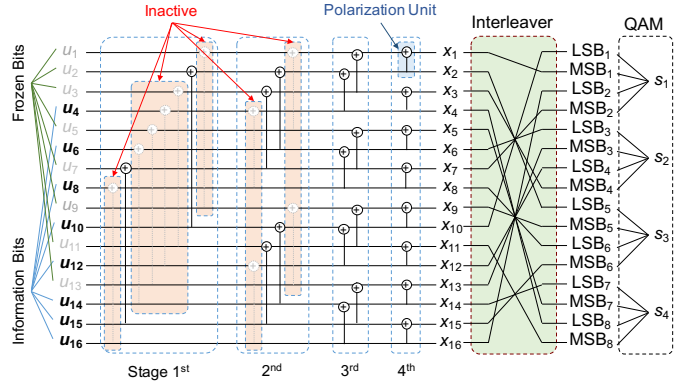

Figure 12. Irregular polar coding with 10 inactivation over 32 total polarization units for BICM.

Polar with irregularity: As for LDPC codes, imposing some sort of irregularity can help improving the performance. Motivated by the fact, we have proposed a new code construction method for irregular polar codes, whose polarization units are irregularly pruned to drastically reduce the computational complexity and decoding latency while achieving better performance.[54] Fig. 12 illustrates an example of irregular polar codes having 10 inactivation over 32 polarization units. Since pruned polarization units do not need any computation for both encoding and decoding, we can reduce the computational complexity. In addition, the decoding latency can be also reduced by carefully choosing the set of inactive polarization units to enable partially parallel computations. This is a great advantage for SCL decoding, which is usually difficult to parallelize. The proposed irregular polar codes showed slightly better performance than regular counterparts while reducing decoding complexity by at least 30 % and decoding latency by 80 %. It was also experimentally demonstrated that the irregular polar codes can outperform the state-of-the-art LDPC codes.[54] We note that the concept of irregular polar codes has more potential by considering various different ways to introduce irregularity not only by pruning.

5. NARROW LINEWIDTH SEMICONDUCTOR LASERS

5.1 Background of narrow linewidth lasers

Narrow linewidth lasers diodes (LDs) are key components for coherent optical communications. There have been numerous research results on semiconductor laser linewidth, both theoretically and experimentally, since 1980s.

The basic theory of LDs was established by introducing the so-called α-parameter.[57] It was then applied to distributed feedback (DFB) lasers,[58] and an additional correction factor for DFB was formulated using Green's functions.[59] Reduction of the α-parameter reduction due to multi-quantum well (MQW) structure was predicted theoretically.[60] The effect of detuned loading (i.e., dispersive external feedback) was also studied.[61] Experimentally, the effect of long cavity DFB lasers,[62] detuning,[63] and MQW DFB lasers,[64] have been verified.

More recently, high power long cavity DFB laser arrays have been used as tunable narrow linewidth lasers.[65,66] Narrow linewidth tunable distributed Bragg reflector (DBR) lasers have also been explored.[67]

Optical feedback can be achieved by capturing a fraction of the output optical power and feeding it back to the laser cavity. This approach is relatively simple and suitable for photonic integration. Owing to the rapid development of photonic integrated circuit (PIC) technology, integrated lasers can be realized monolithically on a single indium phosphide (InP) or with a hybrid integrated platform utilizing an external cavity implementation.[68,69] The former technology is more mature and adequate for near-term deployment, while the latter technology offers lower cost opportunity, although it may require long-term research and development. Here, we describe our recent activity on monolithic integration of optical feedback.

5.2 Integrated laser source with on-chip optical feedback

An integrated InP DBR laser that employs on-chip coherent optical feedback was realized by a standard process in an InP-based multi-project-wafer (MPW) run.[70,71] In order to evaluate the impact of optical feedback on frequency-modulation (FM) noise and linewidth, two type of lasers (Type A and Type B) were designed as shown in Fig. 13 (a) and (b). Type A is a conventional DBR laser, where the laser cavity consists of a high-reflectivity DBR and a 50/50 coupler designed as a broadband partially reflective/partially transmissive mirror. The type B laser is similar but also incorporates a path for optical feedback whereby some light from the 50/50 coupler is fed to the back of the DBR mirror. Fifth-order DBR mirrors are based on side-wall-etched gratings.

Relative intensity noise (RIN) was measured for the two lasers. The lowest peak RIN measured at three different current levels for the Type B laser was -131 dB/Hz at 80 mA. At this pumping current, the RIN for the Type A laser was -117 dB/Hz, indicating a more than 10 dB improvement. The linewidth measurement was conducted using a self-heterodyne method. The linewidth for the Type A laser is 14 MHz and that for the Type B laser is 800 kHz. The RIN reduction qualitatively explains the linewidth reduction. These results indicate that on-chip optical feedback for an integrated InP DBR laser offers a promising approach for further linewidth reduction.
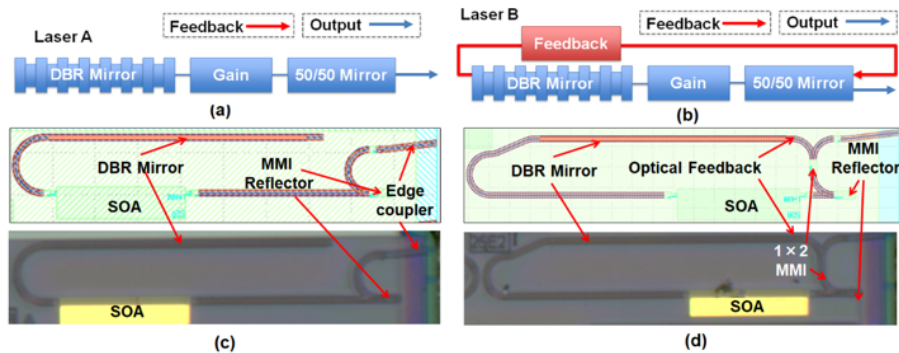

Figure 13. Schematic of the laser cavity design (a) without (Type A) and (b) with (Type B) optical feedback. (c) Layout (top) and microscope image (bottom) of Type A laser. (d) Layout (top) and microscope image (bottom) of Type B laser.[71]

6. CONCLUSION

We have summarized recent progresses in key technology areas in coherent optical communications, including nonlinearity-tolerant multidimensional modulation formats, forward error correction, and narrow linewidth lasers. These technologies are expected to play important roles in higher performance and lower capital and operating expenses in the future optical communication systems.

ACKNOWLEDGMENTS

REFERENCES

[1] Karlsson, M. and Agrell, E., "Which is the most power-efficient modulation format in optical links?," *Optics express* **17**(13), 10814–10819 (2009).

[2] Agrell, E. and Karlsson, M., "Power-efficient modulation formats in coherent transmission systems," *Journal of Lightwave Technology* **27**(22), 5115–5126 (2009).

[3] Millar, D. S., Koike-Akino, T., Kojima, K., and Parsons, K., "Multidimensional modulation for next-generation transmission systems," in [*Proc. of SPIE Vol*], **10130**, 101300E–1 (2017).

[4] Yoshida, T., Matsuda, K., Kojima, K., Miura, H., Dohi, K., Pajovic, M., Koike-Akino, T., Millar, D. S., Parsons, K., and Sugihara, T., "Hardware-efficient precise and flexible soft-demapping for multi-dimensional complementary apsk signals," in [*ECOC 2016; 42nd European Conference on Optical Communication; Proceedings of*], Th.2.P2.SC3.27, VDE (2016).

[5] Millar, D. S., Koike-Akino, T., Arık, S. Ö., Kojima, K., Parsons, K., Yoshida, T., and Sugihara, T., "High-dimensional modulation for coherent optical communications systems," *Optics express* **22**(7), 8798–8812 (2014).

[6] Koike-Akino, T. and Tarokh, V., "Sphere packing optimization and EXIT chart analysis for multi-dimensional QAM signaling," in [*Communications, 2009. ICC'09. IEEE International Conference on*], IEEE (2009).

[7] Cohn, H., Kumar, A., Miller, S. D., Radchenko, D., and Viazovska, M., "The sphere packing problem in dimension 24," *arXiv:1603.06518* (2016).

[8] Hager, C., Amat, A. G. I., Alvarado, A., Brannstrom, F., and Agrell, E., "Optimized bit mappings for spatially coupled LDPC codes over parallel binary erasure channels," in [*Communications (ICC), 2014 IEEE International Conference on*], 2064–2069, IEEE (2014).

[9] Eriksson, T. A., Johannisson, P., Puttnam, B. J., Agrell, E., Andrekson, P. A., and Karlsson, M., "K-over-L multidimensional position modulation," *Lightwave Technology, Journal of* **32**(12), 2254–2262 (2014).

[10] Karlsson, M. and Agrell, E., "Multidimensional modulation and coding in optical transport," *Journal of Lightwave Technology* **35**(4), 876 – 884 (2016).

[11] Shiner, A., Reimer, M., Borowiec, A., Gharan, S. O., Gaudette, J., Mehta, P., Charlton, D., Roberts, K., and O'Sullivan, M., "Demonstration of an 8-dimensional modulation format with reduced inter-channel nonlinearities in a polarization multiplexed coherent system," *Optics express* **22**(17), 20366–20374 (2014).

[12] Kojima, K., Yoshida, T., Koike-Akino, T., Millar, D. S., Parsons, K., and Arlunno, V., "5 and 7 bit/symbol 4D modulation formats based on 2A8PSK," in [*ECOC 2016; 42nd European Conference on Optical Communication; Proceedings of*], W.2.D.1, VDE (2016).

[13] Alvarado, A., Agrell, E., Lavery, D., and Bayvel, P., "LDPC codes for optical channels: Is the "FEC Limit" a good predictor of post-FEC BER," in [*Optical Fiber Commun. Conf.*], Th3E.5, Optical Society of America (2015).

[14] Alvarado, A. and Agrell, E., "Four-dimensional coded modulation with bit-wise decoders for future optical communications," *Journal of Lightwave Technology* **35**(8), 1383–1391 (2017).

[15] Ten Brink, S., Kramer, G., and Ashikhmin, A., "Design of low-density parity-check codes for modulation and detection," *EEE Transactions on Communications* **54**(4), 670–678 (2004).

[16] Bennatan, A. and Bushtein, D., "Design and analysis of nonbinary LDPC codes for arbitrary discrete-memoryless channels," *IEEE Trans. Inf. Theory* **52**(2), 549–583 (2006).

[17] Szczecinski, L. and Alvarado, A., [*Bit-interleaved coded modulation: Fundamentals, analysis, and design*], Wiley, U.K. (2015).

[18] Sugihara, K., Miyata, Y., Sugihara, T., Kubo, K., Yoshida, H., Matsumoto, W., and Mizuochi, T., "A spatially-coupled type LDPC code with an NCG of 12 dB for optical transmission beyond 100 Gb/s," in [*Optical Fiber Communication Conference and Exposition and the National Fiber Optic Engineers Conference (OFC/NFOEC), 2013*], OM2B.4, IEEE (2013).

[19] Poggiolini, P., Bosco, G., Carena, A., Curri, V., and Forghieri, F., "Performance evaluation of coherent WDM PS-QPSK (HEXA) accounting for non-linear fiber propagation effects," *Opt. Exp.* **33**(14), 11360–11371 (2010).

[20] Kojima, K., Yoshida, T., Akino-Koike, T., Millar, D. S., Parsons, K., Pajovic, M., and Arlunno, V., "Nonlinearity-tolerant four-dimensional 2A8PSK family for 5-7 bits/symbol spectral efficiency," *IEEE Journal of Lightwave Technology* **33**(10), 1993–2003 (2017).

[21] Renaudier, J., Voicila, A., Bertran-Pardo, O., Rival, O., Karlsson, M., Charlet, G., and Bigo, S., "Comparison of set-partitioned two-polarization 16QAM formats with PDM-QPSK and PDM-8QAM for optical transmission systems with error-correction coding," in [*European Conf. Optical Communications*], We.1.C.5 (2012).

[22] Pajovic, M., Millar, D. S., Koike-Akino, T., Maher, R., Alvarado, A., Paskov, M., Kojima, K., Parsons, K., Thomsen, B. C., Savory, S. J., et al., "Experimental demonstration of multi-pilot aided carrier phase estimation for DP-64QAM and DP-256QAM," in [*2015 European Conference on Optical Communication (ECOC)*], 1–3, IEEE (2015).

[23] Ishimura, S. and Kikuchi, K., "Fast decoding and LLR-computation algorithms for high-order set-partitioned 4D-QAM constellations," in [*2015 European Conference on Optical Communication (ECOC)*], P.3.01 (2015).

[24] Ishii, K., Dohi, K., Kubo, K., Sugihara, K., Miyata, Y., and Sugihara, T., "A study on power-scaling of triple-concatenated fec for optical transport networks," in [*European Conf. Optical Communications*], Tu3.4.2 (2015).

[25] Zhou, X., Nelson, L., Isaac, R., Magill, P., Zhu, B., Borel, P., Carlson, K., and Peckham, D., "12,000km transmission of 100GHz spaced, 8x495-Gb/s PDM time-domain hybrid QPSK-8QAM signals," in [*Optical Fiber Commun. Conf.*], OTu2B.4, Optical Society of America (2012).

[26] Zhuge, Q., Xu, X., Morsy-Osman, M., Chagnon, M., Qiu, M., and Plant, D., "Time domain hybrid QAM based rate-adaptive optical transmissions using high speed DACs," in [*Optical Fiber Communication Conference/National Fiber Optic Engineers Conference*], *Optical Fiber Communication Conference/National Fiber Optic Engineers Conference 2013*, OTh4E.6, Optical Society of America (2013).

[27] Kojima, K., Yoshida, T., Parsons, K., Koike-Akino, T., Millar, D. S., and Matsuda, K., "Nonlinearity-tolerant time domain hybrid modulation for 4-8 bits/symbol based on 2A8PSK," in [*Optical Fiber Communications Conference and Exhibition (OFC)*], W4A.5, IEEE (2017).

[28] Chung, S. Y., Forney, G. D., Richardson, T. J., and Urbanke, R., "On the design of low-density parity-check codes within 0.0045 dB of the Shannon limit," *IEEE Commun. Lett.* **5**(2), 58–60 (2001).

[29] Koike-Akino, T., Draper, S. C., Wang, Y., Sugihara, K., Matsumoto, W., Millar, D. S., Parsons, K., Arlunno, V., and Kojima, K., "Optimal layered scheduling for hardware-efficient windowed decoding of LDPC convolutional codes," in [*ECOC 2016; 42nd European Conference on Optical Communication; Proceedings of*], W.2.C.2, VDE (2016).

[30] Djordjevic, I. B., "On the irregular nonbinary QC-LDPC-coded hybrid multidimensional OSCD-modulation enabling beyond 100 Tb/s optical transport," *Journal of Lightwave Technology* **31**(16), 2969–2975 (2013).

[31] Koike-Akino, T., Sugihara, K., Millar, D. S., Pajovic, M., Matsumoto, W., Alvarado, A., Maher, R., Lavery, D., Paskov, M., Kojima, K., et al., "Experimental demonstration of nonbinary LDPC convolutional codes for DP-64QAM/256QAM," in [*ECOC 2016; 42nd European Conference on Optical Communication; Proceedings of*], 1–3, VDE (2016).

[32] Xia, T., Koike-Akino, T., Millar, D., Kojima, K., Parsons, K., Miyata, Y., Sugihara, K., and Matsumoto, W., "Nonbinary LDPC convolutional codes for high-dimensional modulations," in [*Signal Processing in Photonic Communications*], SpS3D–5, Optical Society of America (2015).

[33] Koike-Akino, T., Millar, D. S., Kojima, K., Parsons, K., Miyata, Y., Sugihara, K., and Matsumoto, W., "Iteration-aware LDPC code design for low-power optical communications," *Journal of Lightwave Technology* **34**(2), 573–581 (2016).

[34] Koike-Akino, T., Millar, D., Kojima, K., and Parsons, K., "Coded modulation design for finite-iteration decoding and high-dimensional modulation," in [*Optical Fiber Communication Conference*], W4K–1, Optical Society of America (2015).

[35] Richardson, T., Urbanke, R., et al., "Multi-edge type LDPC codes," in [*Workshop honoring Prof. Bob McEliece on his 60th birthday, California Institute of Technology, Pasadena, California*], 24–25 (2002).

[36] Djordjevic, I. B., Xu, L., Wang, T., and Cvijetic, M., "GLDPC codes with Reed-Muller component codes suitable for optical communications," *IEEE Communications Letters* **12**(9) (2008).

[37] Ji, W., Hamaminato, M., Nakayama, H., and Goto, S., "A novel hardware-friendly self-adjustable offset min-sum algorithm for ISDB-S2 LDPC decoder," in [*Signal Processing Conference, 2010 18th European*], 1394–1398, IEEE (2010).

[38] Savin, V. and Declercq, D., "Linear growing minimum distance of ultra-sparse non-binary cluster-LDPC codes," in [*Information Theory Proceedings (ISIT), 2011 IEEE International Symposium on*], 523–527, IEEE (2011).

[39] Wang, Y., Draper, S. C., and Yedidia, J. S., "Hierarchical and high-girth QC LDPC codes," *IEEE Transactions on Information Theory* **59**(7), 4553–4583 (2013).

[40] Zheng, X., Lau, F. C., and Chi, K. T., "Constructing short-length irregular LDPC codes with low error floor," *IEEE Transactions on Communications* **58**(10), 2823–2834 (2010).

[41] Djordjevic, I. B. and Vasic, B., "Projective geometry LDPC codes for ultralong-haul WDM high-speed transmission," *IEEE Photonics Technology Letters* **15**(5), 784–786 (2003).

[42] Yedidia, J. S., Wang, Y., and Draper, S. C., "Divide and concur and difference-map BP decoders for LDPC codes," *IEEE Transactions on Information Theory* **57**(2), 786–802 (2011).

[43] Liu, X., Draper, S. C., and Recht, B., "Suppressing pseudocodewords by penalizing the objective of LP decoding," in [*Information Theory Workshop (ITW), 2012 IEEE*], 367–371, IEEE (2012).

[44] Romero, F. J. C. and Kurkoski, B. M., "Decoding LDPC codes with mutual information-maximizing lookup tables," in [*Information Theory (ISIT), 2015 IEEE International Symposium on*], 426–430, IEEE (2015).

[45] Wei, L., Koike-Akino, T., Mitchell, D. G., Fuja, T. E., and Costello, D. J., "Threshold analysis of non-binary spatially-coupled LDPC codes with windowed decoding," in [*IEEE International Symposium on Information Theory (ISIT)*], 881–885, IEEE (2014).

[46] Casado, A. I. V., Griot, M., and Wesel, R. D., "LDPC decoders with informed dynamic scheduling," *IEEE Transactions on communications* **58**(12), 3470–3479 (2010).

[47] Van Nguyen, T. and Nosratinia, A., "Rate-compatible short-length protograph LDPC codes," *IEEE communications letters* **17**(5), 948–951 (2013).

[48] Sugihara, K., Kametani, S., Kubo, K., Sugihara, T., and Matsumoto, W., "A practicable rate-adaptive FEC scheme flexible about capacity and distance in optical transport networks," in [*Optical Fiber Communications Conference and Exhibition (OFC), 2016*], M.3.A.5, IEEE (2016).

[49] Koike-Akino, T., Kojima, K., Millar, D. S., Parsons, K., Yoshida, T., and Sugihara, T., "Pareto optimization of adaptive modulation and coding set in nonlinear fiber-optic systems," *Journal of Lightwave Technology* **35**(4), 1041–1049 (2017).

[50] Koike-Akino, T., Wang, Y., Draper, S. C., Sugihara, K., Matsumoto, W., Millar, D. S., Parsons, K., and Kojima, K., "Bit-interleaved polar-coded modulation for low-latency short-block transmission," in [*Optical Fiber Communications Conference and Exhibition (OFC), 2017*], W1J.6, Optical Society of America (2017).

[51] Millar, D. S., Koike-Akino, T., Kojima, K., and Parsons, K., "A 24-dimensional modulation format achieving 6 dB asymptotic power efficiency," in [*Signal Processing in Photonic Communications*], SPM3D–6, Optical Society of America (2013).

[52] Millar, D. S., Koike-Akino, T., Maher, R., Lavery, D., Paskov, M., Kojima, K., Parsons, K., Thomsen, B. C., Savory, S. J., and Bayvel, P., "Experimental demonstration of 24-dimensional extended golay coded modulation with LDPC," in [*Optical Fiber Communications Conference and Exhibition (OFC), 2014*], M3A.5, IEEE (2014).

[53] Arikan, E., "Channel polarization: A method for constructing capacity-achieving codes for symmetric binary-input memoryless channels," *IEEE Transactions on Information Theory* **55**(7), 3051–3073 (2009).

[54] Koike-Akino, T., Cao, C., Wang, Y., Draper, S., Millar, D., Parsons, K., Kojima, K., Pajovic, M., Galdino, L., Elson, D., et al., "Irregular polar coding for multi-level modulation in complexity-constrained lightwave systems," in [*ECOC 2017; 43rd European Conference on Optical Communication; Proceedings of*], M.1.D.3, Optical Society of America (2017).

[55] Tal, I. and Vardy, A., "List decoding of polar codes," *IEEE Transactions on Information Theory* **61**(5), 2213–2226 (2015).

[56] Koike-Akino, T., Wang, Y., Draper, S. C., Sugihara, K., and Matsumoto, W., "Bit-interleaved polar-coded OFDM for low-latency M2M wireless communications," in [*Communications (ICC), 2017 IEEE International Conference on*], 1–7, IEEE (2017).

[57] Henry, C., "Theory of the linewidth of semiconductor lasers," *IEEE Journal of Quantum Electronics* **18**, 259–264 (February 1982).

[58] Kojima, K. and Kyuma, K., "Analysis of the spectral linewidth of distributed feedback laser diodes," *Electronics Letters* **20**(21), 869–871 (1984).

[59] Kojima, K. and Kyuma, K., "Analysis of the linewidth of distributed feedback laser diodes using the Green's function method," *Japanese Journal of Applied Physics* **27**(9A), L1721 (1988).

[60] Arakawa, Y. and Yariv, A., "Quantum well lasers–gain, spectra, dynamics," *IEEE Journal of Quantum Electronics* **22**, 1887–1899 (Sep 1986).

[61] Vahala, K. and Yariv, A., "Detuned loading in coupled cavity semiconductor lasers—effect on quantum noise and dynamics," *Applied Physics Letters* **45**(5), 501–503 (1984).

[62] Kojima, K., Noda, S., Tai, S., Kyuma, K., Hamanaki, K., and Nakayama, T., "Long cavity ridge waveguide AlGaAs/GaAs distributed feedback lasers for spectral linewidth reduction," *Applied Physics Letters* **49**(7), 366–368 (1986).

[63] Kojima, K., Noda, S., Tai, S., Kyuma, K., and Nakayama, T., "Measurement of spectral linewidth of AlGaAs/GaAs distributed feedback lasers," *Electronics Letters* **22**(8), 425–427 (1986).

[64] Noda, S., Kojima, K., Kyuma, K., Hamanaka, K., and Nakayama, T., "Reduction of spectral linewidth in AlGaAs/GaAs distributed feedback lasers by a multiple quantum well structure," *Applied Physics Letters* **50**(14), 863–865 (1987).

[65] Kimoto, T., Kobayashi, G., Kurobe, T., Mukaihara, T., and Ralph, S., "Narrow linewidth tunable DFB laser array for PDM-16QAM transmission," in [*18th OptoElectronics and Communications Conference (OECC)*], MK2–6 (June 2013).

[66] Sasahata, Y., Matsumoto, K., Nagira, T., Sakuma, H., Kishimoto, K., Suzuki, M., Suzuki, D., Horiguchi, Y., Takabayashi, M., Mochizuki, K., Gotoda, M., Aruga, H., and Ishimura, E., "Tunable 16 DFB laser array with unequally spaced passive waveguides for backside wavelength monitor," in [*Optical Fiber Communication Conference*], *Optical Fiber Communication Conference* , Th3A.2, Optical Society of America (2014).

[67] Larson, M., Bhardwaj, A., Xiong, W., Feng, Y., dong Huang, X., Petrov, K., Moewe, M., Ji, H., Semakov, A., Lv, C., Kutty, S., Patwardhan, A., Liu, N., Li, Z., Bao, Y., Shen, Z., Bajwa, S., Zhou, F., and Koh, P.-C., "Narrow linewidth sampled-grating distributed Bragg reflector laser with enhanced side-mode suppression," in [*Optical Fiber Communication Conference*], *Optical Fiber Communication Conference* , M2D.1, Optical Society of America (2015).

[68] Song, B., Stagarescu, C., Ristic, S., Behfar, A., and Klamkin, J., "3D integrated hybrid silicon laser," *Opt. Express* **24**(10), 10435–10444 (2016).

[69] Song, B., Liu, Y., Ristic, S., and Klamkin, J., "Tunable 3D hybrid integrated silicon photonic external cavity laser," in [*Conference on Lasers and Electro-Optics (CLEO)*], AM4A.3 (2017).

[70] Song, B., Kojima, K., Koike-akino, T., Wang, B., and Klamkin, J., "Frequency noise reduction of integrated laser source with on-chip optical feedback," in [*Integrated Photonics Research, Silicon and Nanophotonics*], IM3A.4, Optical Society of America (2017).

[71] Song, B., Kojima, K., Pinna, S., Koike-Akino, T., Wang, B., and Klamkin, J., "Noise reduction of integrated laser source with on-chip optical feedback," in [*Asia Communications and Photonics Conference*], M1D.5, Optical Society of America (2017).